


## Article

# Relationship between Young's Modulus and Planar Density of Unit Cell, Super Cells ( $2 \times 2 \times 2$ ), Symmetry Cells of Perovskite ( $\text{CaTiO}_3$ ) Lattice

Marzieh Rabiei <sup>1</sup>, Arvydas Palevicius <sup>1,\*</sup>, Sohrab Nasiri <sup>1,\*</sup>, Amir Dashti <sup>2</sup>, Andrius Vilkauskas <sup>1</sup> and Giedrius Janusas <sup>1,\*</sup>

<sup>1</sup> Faculty of Mechanical Engineering and Design, Kaunas University of Technology, LT-51424 Kaunas, Lithuania; marzieh.rabiei@ktu.edu (M.R.); andrius.vilkauskas@ktu.lt (A.V.)

<sup>2</sup> Department of Materials Science and Engineering, Sharif University of Technology, Tehran 11365-9466, Iran; a.dashty@merc.ac.ir

\* Correspondence: arvydas.palevicius@ktu.lt (A.P.); sohrab.nasiri@ktu.edu (S.N.); giedrius.janusas@ktu.lt (G.J.); Tel.: +370-618-422-04 (A.P.); +370-655-863-29 (S.N.); +370-670-473-37 (G.J.)

**Abstract:** Calcium titanate- $\text{CaTiO}_3$  (perovskite) has been used in various industrial applications due to its dopant/doping mechanisms. Manipulation of defective grain boundaries in the structure of perovskite is essential to maximize mechanical properties and stability; therefore, the structure of perovskite has attracted attention, because without fully understanding the perovskite structure and diffracted planes, dopant/doping mechanisms cannot be understood. In this study, the areas and locations of atoms and diffracted planes were designed and investigated. In this research, the relationship between Young's modulus and planar density of unit cell, super cells ( $2 \times 2 \times 2$ ) and symmetry cells of nano  $\text{CaTiO}_3$  is investigated. Elastic constant, elastic compliance and Young's modulus value were recorded with the ultrasonic pulse-echo technique. The results were  $C_{11} = 330.89$  GPa,  $C_{12} = 93.03$  GPa,  $C_{44} = 94.91$  GPa and  $E = 153.87$  GPa respectively. Young's modulus values of  $\text{CaTiO}_3$  extracted by planar density were calculated 162.62 GPa, 151.71 GPa and 152.21 GPa for unit cell, super cells ( $2 \times 2 \times 2$ ) and symmetry cells, respectively. Young's modulus value extracted by planar density of symmetry cells was in good agreement with Young's modulus value measured via ultrasonic pulse-echo.

**Keywords:** nano-perovskite ( $\text{CaTiO}_3$ ); X-ray diffraction; Young's modulus; ultrasonic-pulse echo; planar density



**Citation:** Rabiei, M.; Palevicius, A.; Nasiri, S.; Dashti, A.; Vilkauskas, A.; Janusas, G. Relationship between Young's Modulus and Planar Density of Unit Cell, Super Cells ( $2 \times 2 \times 2$ ), Symmetry Cells of Perovskite ( $\text{CaTiO}_3$ ) Lattice. *Materials* **2021**, *14*, 1258. <http://doi.org/10.3390/ma14051258>

Academic Editor: Thomas Walter Cornelius and Souren Grigorian

Received: 5 January 2021

Accepted: 2 March 2021

Published: 6 March 2021

**Publisher's Note:** MDPI stays neutral with regard to jurisdictional claims in published maps and institutional affiliations.



**Copyright:** © 2021 by the authors. Licensee MDPI, Basel, Switzerland. This article is an open access article distributed under the terms and conditions of the Creative Commons Attribution (CC BY) license (<https://creativecommons.org/licenses/by/4.0/>).

## 1. Introduction

Perovskites have a general formula of  $\text{ABO}_3$ . In these structures, the A site cation is a typical lanthanide, alkaline or alkaline-earth metal with 12-fold oxygen coordination, and the B-site is any one of a variety of transition metal cations [1]. Calcium titanate ( $\text{CaTiO}_3$ ) was established in 1839 by a Russian mineralogist Perovski, and materials with the same type of  $\text{CaTiO}_3$  were introduced as the perovskite structure.  $\text{CaTiO}_3$  has ionic bonds, as well as the ionic radii of  $\text{Ca}^{2+}$ ,  $\text{O}^{2-}$  and  $\text{Ti}^{4+}$  are 1 Å, 1.40 Å and 0.6 Å, respectively [2]. In recent years, researchers have focused on developing perovskites and their mechanical properties in order to obtain a high yield. Furthermore,  $\text{CaTiO}_3$  is a well-known component in ferroelectric perovskite category, which has been considerably utilized as a dopant/doping in electronic materials due to its dielectric manner and flexibility in structural transformations [3,4]. The modulus of elasticity (E) or Young's modulus is defined as the proportion of the stress to the strain, created by the stress on the body when the body is in the elastic region [5]. The elastic constants are specified from the lattice crystal deformation against force. These elastic moduli are: Young's modulus, shear modulus and volumetric modulus. These modules are registered via inherent elastic properties of materials and their resistance to deformation due to loading. Elastic behavior of materials is described by models such

as Cauchy elastic, hypo-elastic and hyper-elastic. A hyper-elastic is a constitutive model for ideally elastic material that responds against stress gain from a strain energy density function, while for hypo-elastic material, their governing equation is independent of finite strain quantity except in the linearized state [6]. The elastic properties are intimately connected to the crystal structure, the intrinsic character of bonding between the atoms and the anisotropic nature of materials [7,8]; therefore, elastic constants can be derived from crystal lattice calculations [9]. There are several studies on the relationship between elastic constants and planes/directions in a lattice structure, for example, in [10–12]. One of the most accurate methods to measure the elastic stiffness constants and Young's modulus is to determine the velocity of long-wavelength acoustic waves through the ultrasonic pulse-echo technique [13]. In a crystal structure, points, directions and planes are described with an indexing scheme, and planar density is obtained as the number of atoms per unit area, which are centered on a specific crystallographic plane with a defined index [14]. Since the discovery of X-rays at the end of the 19th century, this method has been often used for material characterization [15]. It is used to identify the atomic-scale structure of different materials in a variety of states [16]. X-ray diffraction is the only method that provides the specification of both the mechanical and microstructural character of each diffracted plane. These planes are used as a strain to quantify Young's modulus in one or more planes/directions of the diffraction vector [17]. In forming, designing and manufacturing equipment industries, the use of non-destructive, accurate and convenient methods to determine the mechanical properties of materials is particularly important. Mechanical tests, such as tensile, strike and collision tests, are destructive. Ultrasonic methods are very time-consuming and require operator expertise in this area, and theoretical methods require time-consuming density functional theory (DFT) calculation and may need verification with experimental tests. Our proposed method only needs the XRD analysis, which is a routine test and calculation of planar density; therefore, it can be very significant in terms of industrial application. In this study, the effects of cell size on the accuracy of Young's modulus calculation were considered. Locations of atoms and diffracted planes of unit cell, super cells ( $2 \times 2 \times 2$ ) and symmetry cells of  $\text{CaTiO}_3$  are designed and investigated. The super cell is a cell that describes the same crystal but has a larger volume than a unit cell. By extension of a unit cell proportional to the lattice vectors, the super cells are generated. In super cells ( $2 \times 2 \times 2$ ), the extension is twice of unit cell length in each direction; likewise, for super cells ( $8 \times 8 \times 8$ ), the extension is 8 times. The result extracted by symmetry cells was in good agreement with results recorded via ultrasonic technique. Therefore, this new approach of exploration of reliable Young's modulus quantity based on XRD is proposed for either single crystal or polycrystalline of  $\text{CaTiO}_3$ .

## 2. Experimental

### 2.1. Materials

In this study, for synthesis  $\text{CaTiO}_3$ , titanium (IV) butoxide, calcium chloride dehydrate, sodium hydroxide and ethanol reagents were purchased from Sigma Aldrich (Taufkirchen, Germany) and deionized water as the solvent for dispersions was prepared.

### 2.2. Instrumentation

In this research, a Bruker D8 Advance X-ray diffractometer (Kaunas, Lithuania) with  $\text{CuK}\alpha$  radiation was used. The powder X-ray diffraction was taken at 40 kV and 40 mA, and it was registered at a scanning rate of 2.5 degrees/minute and a step size of 0.02 degrees. The XRD peaks were interpreted by High Score X'Pert software (4.9.0) analysis to get the output ASC type files. The pulse-echo technique was applied for the determination of sound velocity for both transverse and longitudinal ultrasonic signals. For ultrasonic measurement, the model of pulser receiver and oscilloscope were Panametrics Co. (Waltham, MA, USA) and Iwatsu (Tokyo, Japan) (100 MHz), respectively. For powder pressing, the model of mechanical machines was CD04-Z and CIP (CP 360). Additionally, the specific surface area of the sample was investigated by desorption isotherms of nitrogen ( $\text{N}_2$ ) gas

via using a Brunauer-Emmett-Teller (BET) apparatus Gemini V analyzer, micrometrics GmbH (Tehran, Iran). Moreover, transmission electron microscopy (TEM) CM 10-Philips (Tehran, Iran) with acceleration voltage from 50 to 80 KV was utilized.

### 2.3. Methods

#### 2.3.1. Synthesis of Nano-Powder CaTiO<sub>3</sub>

Calcium titanate (CaTiO<sub>3</sub>) was synthesized by solvothermal method. A simple procedure, namely the solvothermal method, was performed for the synthesis of CaTiO<sub>3</sub> (Figure S1). In the first step, (1) calcium chloride dehydrate was stirred with ethanol and deionized water. (2) Titanium (IV) butoxide and ethanol were added to the system drop by drop, under stirring for around 10 min (750 rpm). The molar ratio of ingredients was achieved to calcium chloride dehydrate = 1, ethanol = 5, Titanium (IV) butoxide = 1 and deionized water = 100 respectively. (3) To create pH = 14, sodium hydroxide solution was utilized. (4) The produced solution was placed into the autoclave and the temperature was ~250 °C for 5 h. (5) Afterward, the product was under the drying conditions involved at 110 °C and 0.76 bar, respectively. (6) After a day, the mixture was washed, (7) filtered and dried (110 °C for 4 h), respectively. This method was used in previous studies [18,19].

#### 2.3.2. X-ray Diffraction of CaTiO<sub>3</sub> and Planar Density Calculations

Combining X-ray diffraction of crystalline CaTiO<sub>3</sub> and calculation of planar density values of each diffracted plane was performed. In our study, the atomic density of each plane was considered as the planar density, which was determined as the area of atoms with the center positioned at the plane divided by the total area of the plane, and it is a determinant factor for mechanical properties of each plane. Planar density is a unitless parameter, and its value is less than 1 in each cell. Furthermore, the values of planar density are related to the positions and situations of atoms in the planes. For determination of atomic area, the Crystal Maker, Version 10.2.2 software was performed. First of all, the three-dimensional (3D) geometry of crystal structures was designed, and then, from the intersection area of each diffracted plane with atoms located at the plane, the atomic area was calculated. When an atom with diameter  $D$  was involved completely, the atomic area will be  $A = \pi\left(\frac{D}{2}\right)^2$ ; otherwise, it will be a percentage of this amount.

#### 2.3.3. Ultrasonic Pulse-Echo Technique of CaTiO<sub>3</sub>

An ultrasonic wave is a type of elastic wave spread in the medium with high frequency to obtain the Young's modulus value of samples. Mastering the ultrasonic parameters can be used to acquire more accurate values of mechanical properties [20]. Recently, different studies on mechanical properties have been done by ultrasonic techniques. Basically, the crossing of longitudinal and transverse waves in nano- or microstructures is performed at different velocities. Each returned velocity is considered as the represented properties.

For ultrasonic measurements based on the Christoffel procedure, the first cubic specimen of CaTiO<sub>3</sub> was prepared by cold isostatic press. The schematics of ultrasonic measurement are depicted in Figure 1a. The main part of the ultrasonic system is the pulser-receiver, which creates an electric pulse and stimulates the probe. Furthermore, the produced pulses enter the specimen, and after a sweep, they can be received via a probe. In this measurement, some drops of water were utilized to prevent the depreciation of waves in the air, and the effect of hand pressure on the probe was decreased [21].

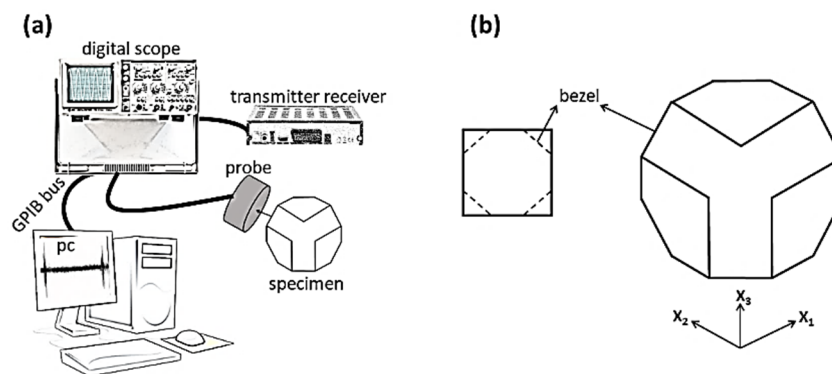


**Figure 1.** Schematic of (a) ultrasonic pulse instrument and (b) a sketch of prepared  $\text{CaTiO}_3$  sample.

At any position in the sample, a local coordinate is adjusted, such as  $X_1$ , the radial coordinate;  $X_2$ , the circumferential coordinate; and  $X_3$ , the axial coordinate.  $V_{i/j}$  denotes the velocity of an ultrasound wave propagating in the  $X_i$  direction with particle displacements in the  $X_j$  direction.  $V_{i/j}$  with the same  $i$  and  $j$  is longitudinal, and with  $i \neq j$  is related to the transverse waves. For the measurement of quasi-longitudinal or quasi-transverse velocity ( $V_{ij/ij}$ ), the specimen should be cut (bezel) on the edges of the surfaces perpendicular to the  $X$  directions. A sketch of the sample is represented in Figure 1b.

### 3. Results

#### 3.1. X-ray Diffraction of $\text{CaTiO}_3$ and Planar Density Calculations

The XRD pattern of  $\text{CaTiO}_3$  is presented in Figure 2. The characteristic peaks of  $\text{CaTiO}_3$  correspond to the report in Ref [22]. The crystal structure of  $\text{CaTiO}_3$  is cubic, the atomic positions of Ti are at (000), Ca at  $(\frac{1}{2}, \frac{1}{2}, \frac{1}{2})$  and O at  $(\frac{1}{2}, 0, 0)$ ,  $(0, \frac{1}{2}, 0)$ ,  $(0, 0, \frac{1}{2})$ . According to X-ray powder diffraction results, the lattice parameter is  $3.79 \pm 0.02 \text{ \AA}$ , which is in good corresponds with the amount recorded in the Ref [23]. In addition, crystallographic parameters (Table S1) of  $\text{CaTiO}_3$  and analyzed data by X'Pert [24] nasiri are recorded as the cell volume =  $54.44 \pm 0.01 \text{ \AA}^3$  and crystal density =  $4.14 \pm 0.01 \text{ g/cm}^3$ , and the space group is Pm-3m. In addition, the crystal size of  $\text{CaTiO}_3$  was calculated by the Monshi-Scherrer equation (Figure S2) [25] and BET analysis. The crystal size values were registered at  $\sim 59.10$  and  $63.02 \text{ nm}$ , respectively. The Monshi-Scherrer method is described in Section 2 of the supporting information. Furthermore, a TEM image of  $\text{CaTiO}_3$  is shown in Figure S3. According to the images shown in Figure S3, the size of  $\text{CaTiO}_3$  particles basically corresponds to the crystallite size, and it is clear that particles of powder have nanoscale and size can be reported almost  $\pm 50 \text{ nm}$ .

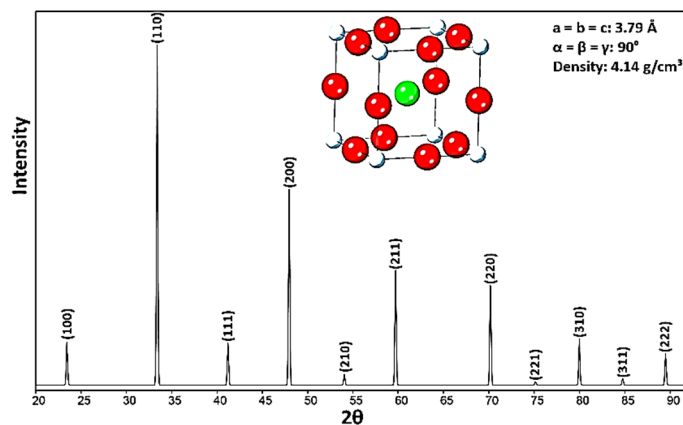
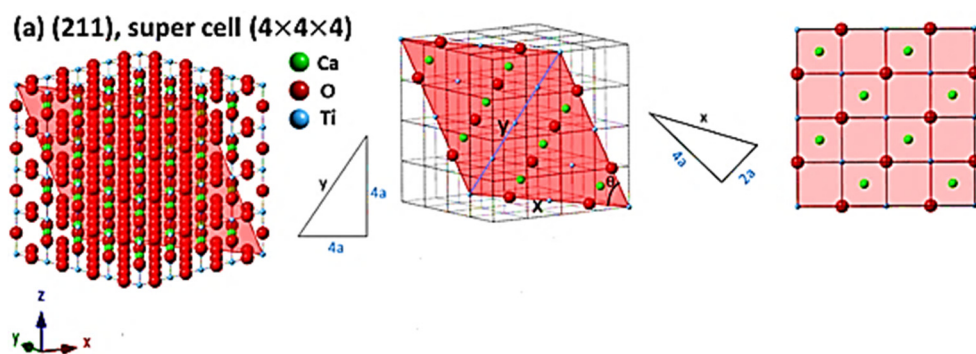


**Figure 2.** X-ray diffraction of  $\text{CaTiO}_3$  (powder sample).



For the evaluation of cells as the results, the comprehensive calculations of the planar density of diffracted planes in the unit cell, super cells (2 × 2 × 2) and super cells (8 × 8 × 8) of CaTiO<sub>3</sub> lattice are presented in Figures S4–S6 respectively. In addition, the locations of atoms, geometry of planes and calculations of planar density of (211) super cell (4 × 4 × 4), (211) super cell (8 × 8 × 8), (221) super cell (4 × 4 × 4), (221) super cell (8 × 8 × 8), (311) super cell (3 × 3 × 3), (311) super cell (4 × 4 × 4), (311) super cell (8 × 8 × 8), (222) super cell (3 × 3 × 3) and (222) super cell (8 × 8 × 8) are depicted briefly in Figures 3–6 respectively. Furthermore, the completed calculations with their figures are shown in Figures S7–S10.



number of atoms in the plane (211) × area of each atom in the plane (211) =

$$\left[ \left( 2 \times \frac{78.52}{360} + 2 \times \frac{101.48}{360} + 4 \times \frac{1}{2} + 5 \right) \times \pi (r_{Ti^{++}})^2 \right] + \left[ \left( 8 \times \frac{1}{2} + 4 \right) \times \pi (r_{O^{2-}})^2 \right] + \left[ 8 \times \pi (r_{Ca^{+}})^2 \right] =$$

$$\left[ (8 \times \pi (0.60)^2) + (8 \times \pi (1.40)^2) + (8 \times \pi (1)^2) \right] = 83.44$$

$$\text{Planar density} = \frac{\text{number of atoms in the plane (211)} \times \text{area of each atom in the plane (211)}}{\text{area of the plane (211)}} = \frac{83.44}{334.1} = 0.25$$

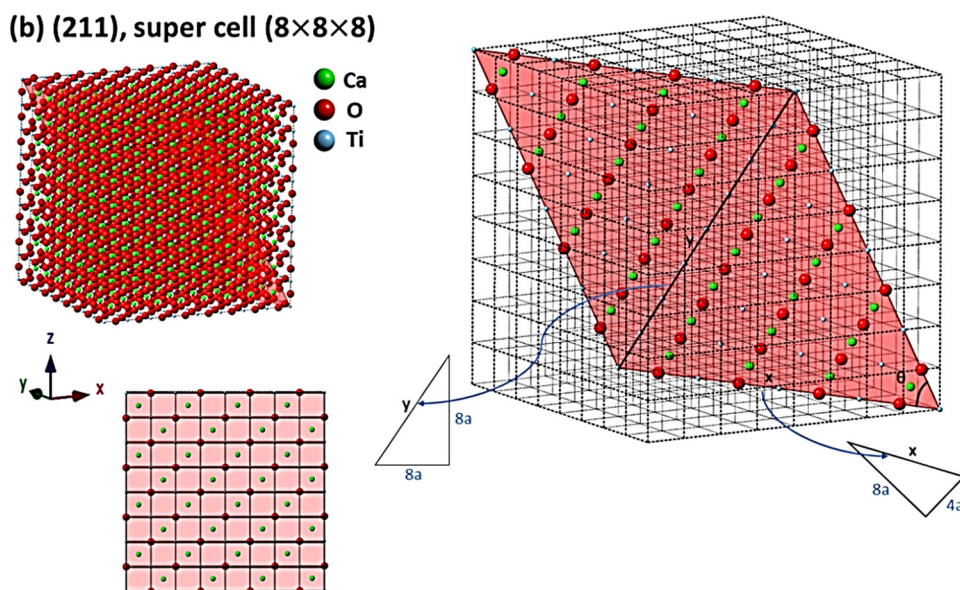


Figure 3. Cont.

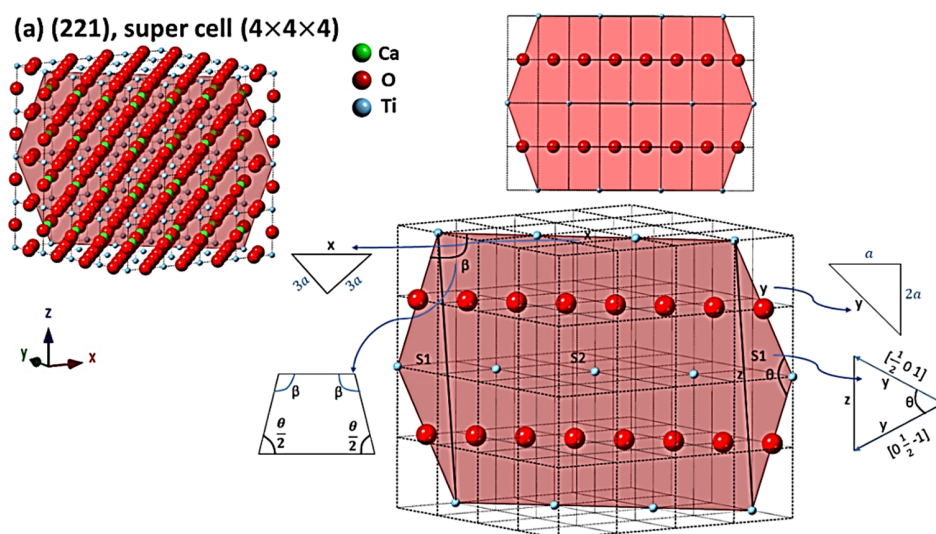
number of atoms in the plane (211) × area of each atom in the plane (211) =

$$\left[ \left( 2 \times \frac{78.52}{360} + 2 \times \frac{101.48}{360} + 12 \times \frac{1}{2} + 25 \right) \times \pi (r_{Ti^{4+}})^2 \right] + \left[ \left( 16 \times \frac{1}{2} + 24 \right) \times \pi (r_{O^{2-}})^2 \right] + \left[ \left( 32 \times \pi (r_{Ca^{+}})^2 \right) \right] =$$

$$\left[ \left( 32 \times \pi (0.60)^2 \right) + \left( 32 \times \pi (1.40)^2 \right) + \left( 32 \times \pi (1)^2 \right) \right] = 333.76$$

$$\text{Planar density} = \frac{\text{number of atoms in the plane (211)} \times \text{area of each atom in the plane (211)}}{\text{area of the plane (211)}} = \frac{333.76}{1335.24} = 0.25$$

**Figure 3.** Geometry of planes and calculations of planar density of (a) (211) super cell (4 × 4 × 4) and (b) (211) super cell (8 × 8 × 8) (which shows and emphasizes the symmetry of (8 × 8 × 8) super cells).



number of atoms in the plane (221) × area of each atom in the plane (221) =

$$\left[ \left( 2 \times \frac{143.13}{360} + 4 \times \frac{108.44}{360} + 4 \times \frac{1}{2} + 3 \right) \times \pi (r_{Ti^{4+}})^2 \right] + \left[ \left( 12 + 4 \times \frac{1}{2} \right) \times \pi (r_{O^{2-}})^2 \right] = \left[ \left( 7 \times \pi (0.60)^2 \right) + \left( 14 \times \pi (1.40)^2 \right) \right] = 94.12$$

$$\text{Planar density} = \frac{\text{number of atoms in the plane (221)} \times \text{area of each atom in the plane (221)}}{\text{area of the plane (221)}} = \frac{94.12}{301.71} = 0.31$$

**(b) (221), super cell (8 × 8 × 8)**

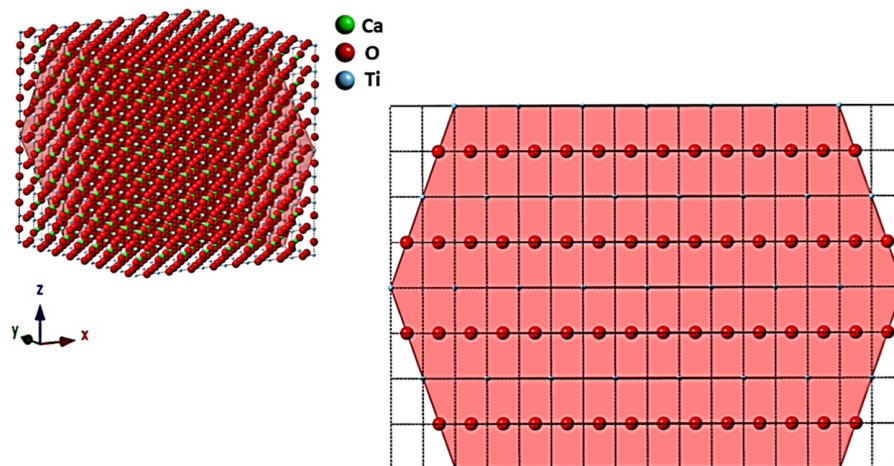
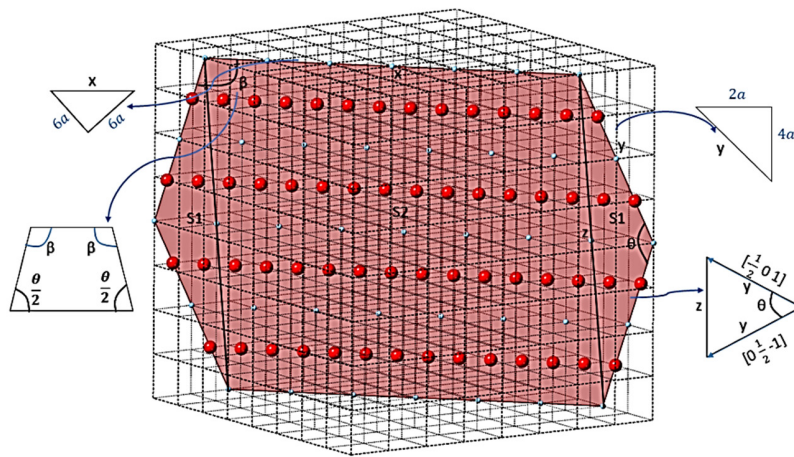


**Figure 4.** Cont.

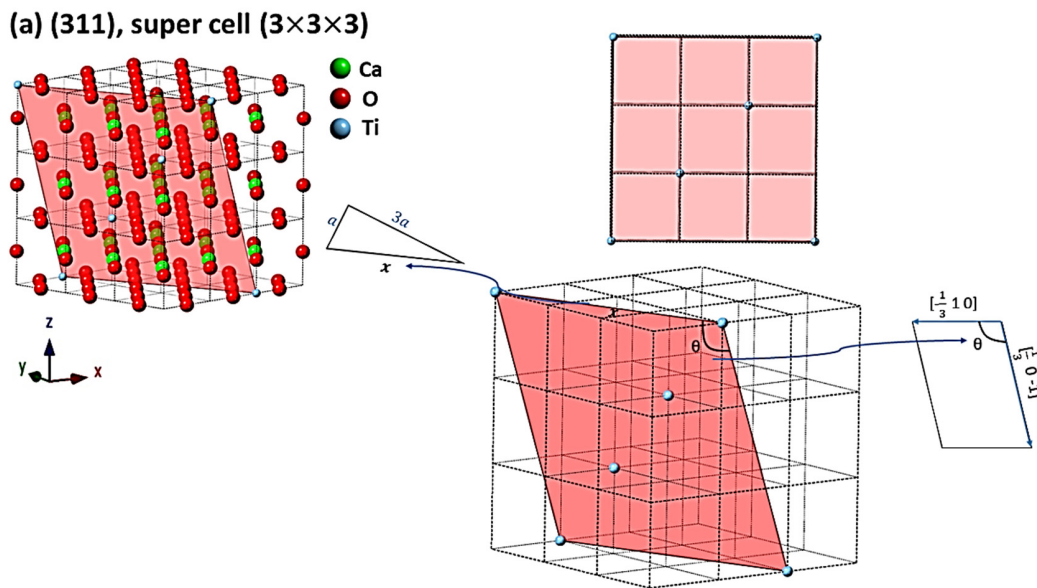


number of atoms in the plane (221)  $\times$  area of each atom in the plane (221) =

$$\left[ \left( 2 \times \frac{143.13}{360} + 4 \times \frac{108.44}{360} + 14 \times \frac{1}{2} + 19 \right) \times \pi (r_{Ti^{4+}})^2 \right] + \left[ \left( 52 + 8 \times \frac{1}{2} \right) \times \pi (r_{O^{2-}})^2 \right] = [28 \times \pi (0.60)^2 + (56 \times \pi (1.40)^2)] = 376.49$$

$$\text{Planar density} = \frac{\text{number of atoms in the plane (221)} \times \text{area of each atom in the plane (221)}}{\text{area of the plane (221)}} = \frac{376.49}{1206.65} = 0.31$$

**Figure 4.** Geometry of planes and calculations of planar density of (a) (221) super cell (4  $\times$  4  $\times$  4) and (b) (221) super cell (8  $\times$  8  $\times$  8) (which shows and emphasizes the symmetry of (8  $\times$  8  $\times$  8) super cells).



number of atoms in the plane (311)  $\times$  area of each atom in the plane (311) =

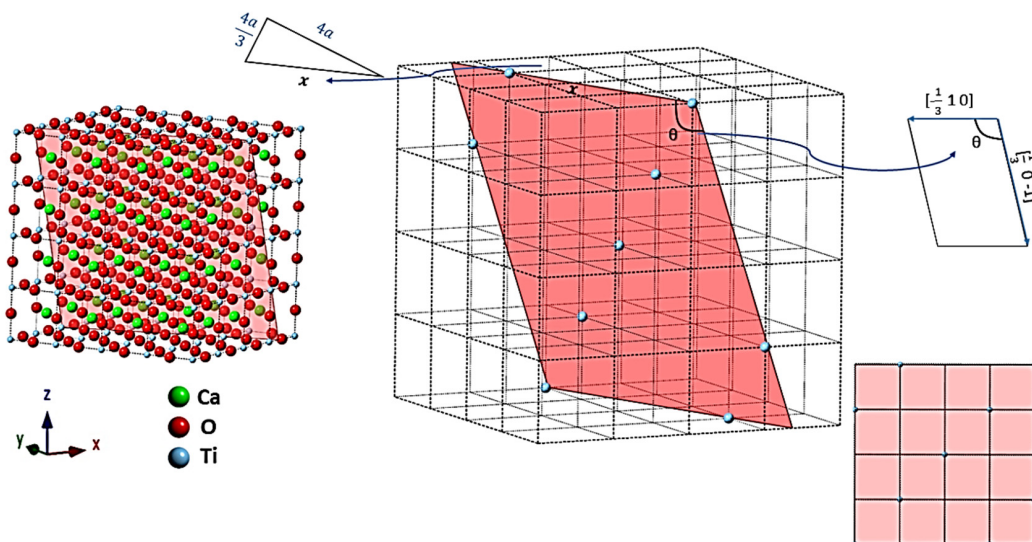
$$\left[ \left( 2 \times \frac{95.74}{360} + 2 \times \frac{84.26}{360} + 2 \right) \times \pi (r_{Ti^{4+}})^2 \right] = (3 \times \pi \times (0.6)^2) = 3.39$$

$$\text{Planar density} = \frac{\text{number of atoms in the plane (311)} \times \text{area of each atom in the plane (311)}}{\text{area of the plane (311)}} = \frac{3.39}{143.04} = 0.02$$

**Figure 5.** Cont.



**(b) (311), super cell (4×4×4)**

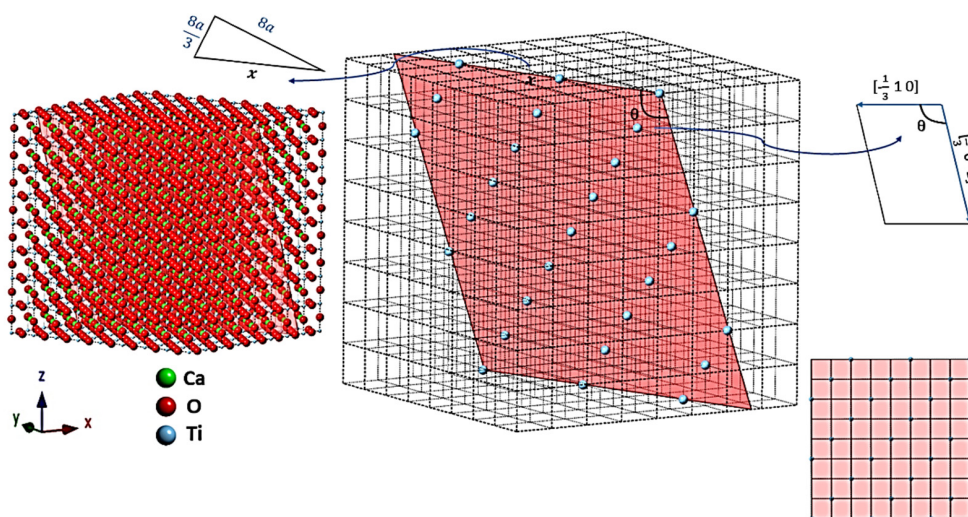


number of atoms in the plane (311) × area of each atom in the plane (311) =

$$\left[ \left( 2 \times \frac{95.74}{360} + 4 \times \frac{1}{2} + 3 \right) \times \pi (r_{\text{Ti}^{++}})^2 \right] = (5.53 \times \pi \times (0.6)^2) = 6.25$$

$$\text{Planar density} = \frac{\text{number of atoms in the plane (311)} \times \text{area of each atom in the plane (311)}}{\text{area of the plane (311)}} = \frac{6.25}{254.40} = 0.02$$

**(c) (311), super cell (8×8×8)**



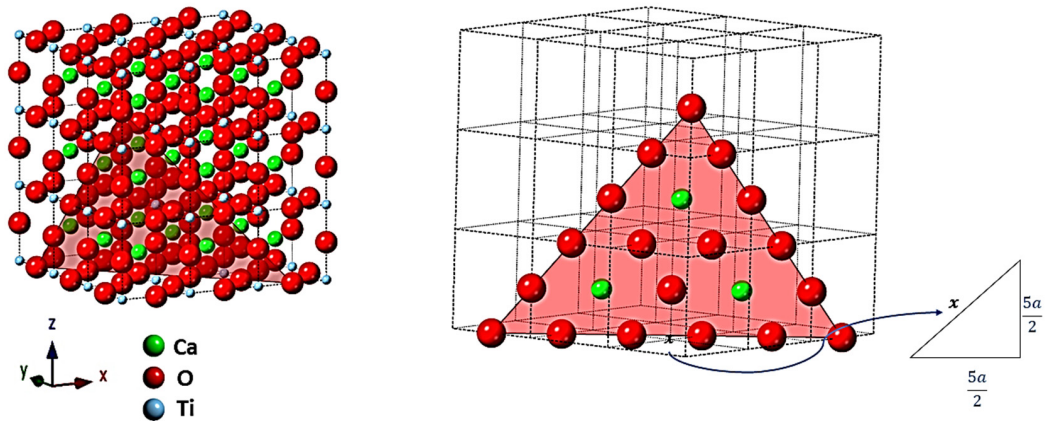
number of atoms in the plane (311) × area of each atom in the plane (311) =

$$\left[ \left( 2 \times \frac{95.74}{360} + 8 \times \frac{1}{2} + 17 \right) \times \pi (r_{\text{Ti}^{++}})^2 \right] = (21.53 \times \pi \times (0.6)^2) = 24.35$$

$$\text{Planar density} = \frac{\text{number of atoms in the plane (311)} \times \text{area of each atom in the plane (311)}}{\text{area of the plane (311)}} = \frac{24.35}{1016.32} = 0.02$$

**Figure 5.** The concept of a symmetry cell; geometry of planes and calculations of planar density of (a) (311) super cell (3 × 3 × 3), (b) (311) super cell (4 × 4 × 4) and (c) (311) super cell (8 × 8 × 8).

(a) (222), super cell (3×3×3)

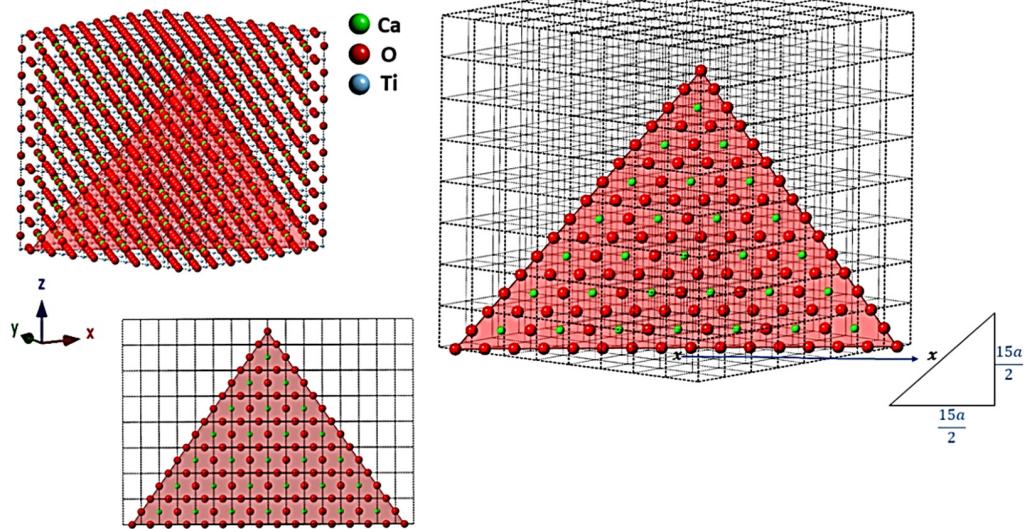


$$\text{number of atoms in the plane (222)} \times \text{area of each atom in the plane (222)} = \left[ \left( 3 \times \frac{1}{6} + 12 \times \frac{1}{2} + 3 \right) \times \pi (r_{O^{2-}})^2 \right] + \left[ 3 \times \pi (r_{Ca^{+}})^2 \right] =$$

$$[(9.5 \times \pi (1.40)^2)] + [(3 \times \pi (1)^2)] = 67.92$$

$$\text{Planar density} = \frac{\text{number of atoms in the plane (222)} \times \text{area of each atom in the plane (222)}}{\text{area of the plane (222)}} = \frac{67.92}{77.28} = 0.88$$

(b) (222), super cell (8×8×8)



$$\text{number of atoms in the plane (222)} \times \text{area of each atom in the plane (222)} = \left[ \left( 3 \times \frac{1}{6} + 42 \times \frac{1}{2} + 63 \right) \times \pi (r_{O^{2-}})^2 \right] + \left[ 28 \times \pi (r_{Ca^{+}})^2 \right] =$$

$$[(84.5 \times \pi (1.40)^2)] + [(28 \times \pi (1)^2)] = 608.28$$

$$\text{Planar density} = \frac{\text{number of atoms in the plane (222)} \times \text{area of each atom in the plane (222)}}{\text{area of the plane (222)}} = \frac{608.28}{695.92} = 0.88$$

Figure 6. Geometry of planes and calculations of planar density of (a) (222) super cell (3 × 3 × 3) and (b) (222) super cell (8 × 8 × 8).



### 3.2. Investigation of Results Obtained from Ultrasonic Pulse-Echo Technique of CaTiO<sub>3</sub>

Taking into account the Christoffel equation, the connection between ultrasonic phase velocity and the stiffness matrix is given as follows:

$$\left( C_{ijkl}l_jl_l - \rho V^2 \delta_{ik} \right) \alpha_k = 0$$

where  $V$  is the ultrasonic phase velocity,  $C_{ijkl}$  is the general stiffness matrix,  $\rho$  is the material density,  $l$  is the orientation of propagation,  $\alpha_k$  is the polarization direction and  $\delta_{ik}$  is the Kronecker delta (note that  $i, j, k, l = 1$  to  $3$ ). For the extraction and calculation of elastic constants from ultrasonic measurements based on the Christoffel equation, with the propagation in  $X_1, X_2$  and  $X_3$  directions, all of the diagonal elements of the stiffness matrix are obtained. For the determination of whole constants, we cut the specimen on the edges of the surfaces perpendicular to principal directions (bezel) and the velocity was measured from the propagation of ultrasound wave normal to these planes.

Based on Equations (1)–(5) [26,27] and the measured velocity according to the Table 1, stiffness constants values were obtained.  $C_{11}$  is in the agreement with longitudinal distortion and longitudinal compression/tension, so  $C_{11}$  can be described as the hardness. Moreover, the transverse distortion is connected to the  $C_{12}$ , and  $C_{12}$  is obtained from the transverse expansion correlated to the Poisson's ratio.  $C_{44}$  is based on the shear modulus, as well as  $C_{44}$  is in the settlement with  $C_{11}$  and  $C_{12}$  [26].

$$C_{11} = \rho V_1^2 \quad (1)$$

$$C_{22} = \rho V_2^2 \quad (2)$$

$$C_{66} = \rho V_{\frac{1}{2}}^2 = \rho V_{\frac{2}{1}}^2 \quad (3)$$

$$C_{12} = \sqrt{(C_{11} + C_{66} - 2\rho V_{\frac{12}{12}}^2)(C_{22} + C_{66} - 2\rho V_{\frac{12}{12}}^2)} - C_{66} \quad (4)$$

$$C_{44} = \rho V_{\frac{2}{3}}^2 = \rho V_{\frac{3}{2}}^2 \quad (5)$$

**Table 1.** The values of longitudinal and transverse velocity of the sample.

Longitudinal Velocity (m/s)	Transverse Velocity (m/s)	Quasi Longitudinal or Quasi Transverse (m/s)
$V_{1/1} = 9261.85$ $V_{2/2} = 8013.51$	$V_{2/3} = 4960.5$ $V_{1/2} = 4283.65$	$V_{12/12} = 4976.63$

After substitution and calculation,  $C_{11}, C_{12}$  and  $C_{44}$  were registered at 330.89, 93.03 and 94.91 GPa respectively. These values of CaTiO<sub>3</sub> were in good agreement with the values submitted in the [28–30]. Moreover, with the ultrasonic technique, longitudinal and transverse waves can be utilized for determining Young's modulus quantity [31,32]. The longitudinal and transverse waves of CaTiO<sub>3</sub> sample are shown in Figure 7. In this method, by measuring the waves velocity and density of specimen, the determination of Young's modulus quantity was carried out (Equation (6)).

$$E = \frac{4\rho \left( \frac{L}{t_s} \right)^2 (3t_s^2 - 4t_l^2)}{t_s^2 - t_l^2} \quad (6)$$

where,  $t_s$  and  $t_l$  are differences between two echo in longitudinal and transverse waves, respectively [33,34]. According to the results shown in Figure 7,  $t_s$  and  $t_l$  values are calculated as 5.75 and 3.01  $\mu$ s, respectively. In addition, the density of the specimen is recorded as 3857.30  $\frac{\text{Kg}}{\text{m}^3}$ , and the length of the specimen after powder pressing reached 11.21 mm. After

calculation, Young's modulus value of CaTiO<sub>3</sub> was 153.87 GPa. This value corresponds with the value reported by Ramajo et al. [35].

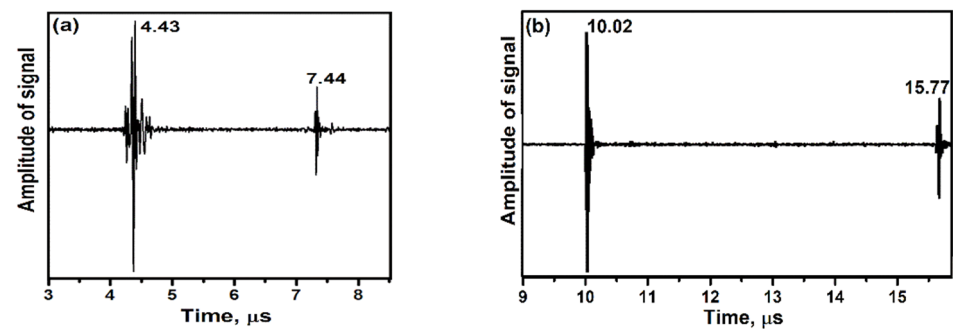


**Figure 7.** Recorded signals extracted via (a) longitudinal waves and (b) transverse waves of CaTiO<sub>3</sub> specimen.

### 3.3. Calculations: Relationship between Elastic Stiffness–Compliance Constants, Young's Modulus and Planar Density Extracted through the Unit Cell, Super Cells (2 × 2 × 2) and Symmetry Cells of CaTiO<sub>3</sub> Lattice

Three elastic constants of CaTiO<sub>3</sub> were calculated via the ultrasonic technique. For the cubic CaTiO<sub>3</sub> system, the relationship between stiffness ( $C_{ij}$ ) and compliance constant ( $S_{ij}$ ) are provided in Equations (7)–(9) [27,36]. The values resulted via Equations (7)–(9) are 0.0034, −0.0007 and 0.0105 GPa for  $S_{11}$ ,  $S_{12}$  and  $S_{44}$ , respectively. Furthermore, Young's modulus of each diffracted plane of CaTiO<sub>3</sub> can be written as Equation (10) [37].

$$S_{11} = \frac{C_{11} + C_{12}}{(C_{11} - C_{12})(C_{11} + 2C_{12})} \quad (7)$$

$$S_{12} = \frac{-C_{12}}{(C_{11} - C_{12})(C_{11} + 2C_{12})} \quad (8)$$

$$S_{44} = \frac{1}{C_{44}} \quad (9)$$

$$\frac{1}{E_{hkl}} = S_{11} - 2 \left[ (S_{11} - S_{12}) - \frac{1}{2} S_{44} \right] \left[ \frac{h^2 k^2 + k^2 l^2 + l^2 h^2}{(h^2 + k^2 + l^2)} \right] \quad (10)$$

The planar density and Young's modulus values related to the each diffracted plane of the unit, super (2 × 2 × 2), symmetry and super (8 × 8 × 8) cells of CaTiO<sub>3</sub> lattice are tabulated in Table 2.

**Table 2.** Planar density and Young's modulus values of the unit cell, super cells (2 × 2 × 2) and symmetry cells of CaTiO<sub>3</sub>.

Index	Planar Density of Unit Cell	Planar Density of Super Cell (2 × 2 × 2)	Planar Density of Symmetry Cells	Planar Density of Super Cell (8 × 8 × 8)	Young's Modulus (GPa)
(100)	0.93	0.93	0.93 in (2 × 2 × 2)	0.93	290.059
(110)	0.51	0.51	0.51 in (2 × 2 × 2)	0.51	221.652
(111)	0.04	0.04	0.04 in (2 × 2 × 2)	0.04	179.354
(200)	0.64	0.64	0.64 in (2 × 2 × 2)	0.64	290.059
(210)	0.41	0.41	0.41 in (2 × 2 × 2)	0.41	194.176
(211)	0.16	0.25	0.25 in (2 × 2 × 2)	0.25	150.612
(220)	0.6	0.6	0.6 in (2 × 2 × 2)	0.6	129.810
(221)	0.46	0.29	0.31 in (4 × 4 × 4)	0.31	109.622
(310)	0.24	0.24	0.23 in (4 × 4 × 4)	0.23	186.471
(311)	0.04	0.03	0.02 in (3 × 3 × 3)	0.02	140.386
(222)	0.99	0.88	0.88 in (3 × 3 × 3)	0.88	83.615

#### 4. Discussion

According to Table 2 and Figures 3–6, the expanded cells have an optimum matrix, and in this case, achieving the optimum matrix is introduced as the symmetry cells. An optimum matrix is the minimum extension for a specific plane of the unit cell to a super cell from which the density plane of that plane does not change. For example, symmetry cell (optimum matrix) of (311) plane is  $(3 \times 3 \times 3)$ , which means that after extending to a greater matrix such as  $(4 \times 4 \times 4)$  or  $(8 \times 8 \times 8)$ , planar density values will be similar (Figure 5a–c). Real planar density values of each plane are obtained from the symmetry cell, because once the symmetry of each plane is reached, with the extension of that plane to infinity (real plane), the planar density does not change. In addition, to recognize the symmetry cell, knowing some parameters such as crystal lattice, locations of atoms in the planes and index of planes is essential. Therefore, to determine Young's modulus values based on the planar density of  $\text{CaTiO}_3$ , the symmetry cells should be found. It is very interesting that symmetrical or real values are related to the super cells of the  $(8 \times 8 \times 8)$  matrix, because in matrix  $(8 \times 8 \times 8)$ , lattice correspondence in all directions is available; therefore, real planar density values should be calculated for the super cell of  $(8 \times 8 \times 8)$  matrix. To confirm this, calculations of real planar density and geometry of atoms and planes of (211), (221), (311) and (222) in super cells  $(8 \times 8 \times 8)$  are presented in Figures 3b, 4b, 5c and 6b, respectively. It is clear that finding the exact situation of planes and geometries is sophisticated, but with when they are known, the results obtained from Young's modulus values will have fewer errors. The basic supposition is that when the planar density is raised, the motion of atoms with the mechanism of dislocation movement needs high forces. Dislocations are regions in the lattice where an additional plane of atoms have been included abstracted from an ideal crystal (without imperfections). Dislocations are caused by losing acoustic energy, and this matter will affect the values of wavelength and time of ultrasonic waves [38].

The force ( $W$ ), which is needed for the movement of atoms in each plane, is obtained from Equation (11) [39].

$$W = \frac{E}{2(1 + \nu)} b^2 l \quad (11)$$

In Equation (11),  $E$  is Young's modulus,  $b$  is Burgers vector,  $l$  is dislocation length and  $\nu$  is Poisson's ratio. The higher value of force is in accordance with the modulus of elasticity (Young's modulus), which would be higher.

To compare Young's modulus values of  $\text{CaTiO}_3$  in a unit cell, super cells  $(2 \times 2 \times 2)$  and symmetry cells, the fitting of Young's modulus values extracted by each diffracted plane versus planar density values is presented in Figure 8. According to the results (shown in the Figure 8) and the straight fitting line, Young's modulus values of unit cell, super cells  $(2 \times 2 \times 2)$  and symmetry cells were calculated as  $162.62 \pm 0.4$  GPa,  $151.71 \pm 0.4$  GPa and  $152.21 \pm 0.4$  GPa, respectively. As expected, the Young's modulus value of symmetry cells of  $\text{CaTiO}_3$  ( $152.21 \pm 0.4$  GPa) is in good agreement with experimental Young's modulus value extracted via ultrasonic-echo technique ( $153.87 \pm 0.2$  GPa). Moreover, Young's modulus value of unit cell ( $162.62 \pm 0.4$  GPa) has a greater difference with experimental Young's modulus value, and as a result, the unit cell of  $\text{CaTiO}_3$  cannot be represented as whole cells. This is because in a unit cell of  $\text{CaTiO}_3$ , crystalline defects are not considered and is especially controlling of deformation, and displacement of atoms in the planes is related to the dislocation networks [40]. Further, a unit cell of  $\text{CaTiO}_3$  is not involved in imperfections (such as dislocations, Frenkel defect and Schottky defect) with respect to the super cell [41]; therefore, the slope line value of the unit cell is reported (37.23) to be less than the slope line value of super cells  $(2 \times 2 \times 2)$  (63.67) and symmetry cells (62.41). Consequently, the effect of imperfections in expanded cells (super cells) is very impressive, so the unit cell of  $\text{CaTiO}_3$  is considered as the ideal lattice, while symmetry cells such as  $(8 \times 8 \times 8)$  of  $\text{CaTiO}_3$  are real lattices [42]; this is consistent with the experimental Young's modulus. It is clear that each imperfection will be caused by a decreasing Young's modulus [43], and in Figure 8, this matter is confirmed when the Young's modulus value (intercept) in the unit cell of  $\text{CaTiO}_3$  is higher than in super cells  $(2 \times 2 \times 2)$  and symmetry cells. Apparently, a

unit cell of  $\text{CaTiO}_3$  is represented by the volume of a real crystal, so the unit cell is useful to acquire theoretical density. Nevertheless, calculations of planar density based on the unit cell were obtained, but with errors.

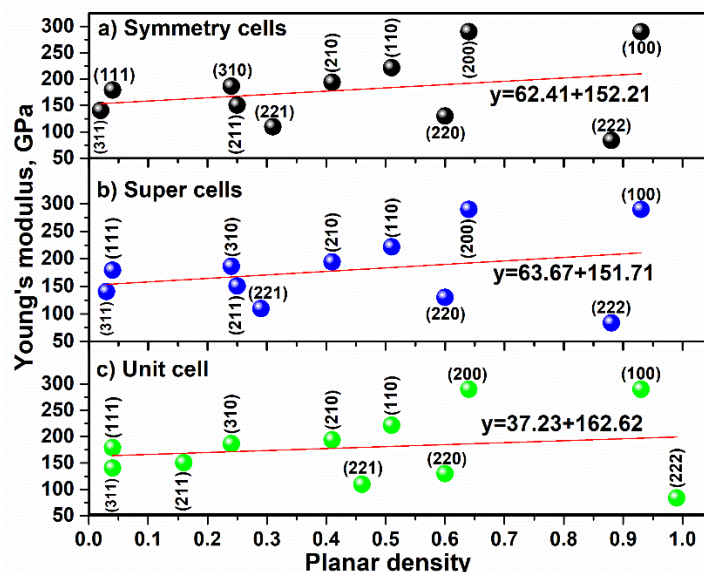


**Figure 8.** Young's modulus versus planar density values of each diffracted plane related to the (a) symmetry cells, (b) super cells ( $2 \times 2 \times 2$ ) and (c) unit cell of  $\text{CaTiO}_3$ .

## 5. Conclusions

1.  $\text{CaTiO}_3$  as a category of perovskite is successfully synthesized via solvothermal method.
2. Crystal size values of  $\text{CaTiO}_3$  are calculated as  $\sim 59.10$  and  $63.02$  through the Monshi-Scherrer method and BET analysis, and the crystal size values were confirmed by TEM image.
3. Planar density is responsible for modulus of elasticity of that plane; therefore, for the first time, comprehensive calculations of geometry, location and planar density values of  $\text{CaTiO}_3$  were shown.
4. Elastic stiffness constants and Young's modulus values of  $\text{CaTiO}_3$  were obtained by ultrasonic-echo method ( $C_{11} = 330.89$ ,  $C_{12} = 93.03$ ,  $C_{44} = 94.91$  GPa and  $E = 153.87 \pm 0.2$  GPa).
5. Young's modulus values of  $\text{CaTiO}_3$  extracted by planar density and least square method were calculated as  $162.62 \pm 0.4$ ,  $151.71 \pm 0.4$  and  $152.21 \pm 0.4$  GPa for unit cell, super cells ( $2 \times 2 \times 2$ ) and symmetry cells, respectively.
6. The Young's modulus value of  $\text{CaTiO}_3$  reported by symmetry cells is in good agreement with Young's modulus value reported by ultrasonic-echo technique and the literature.
7. A unit cell of  $\text{CaTiO}_3$  is not representative of the distribution of atoms on the planes; therefore, to obtain the real value of planar density and find the symmetry of distribution of atoms on the planes, expanded cells and utilizing symmetry cells are suggested.
8. Obtaining the planar density values based on unit cell or each super cells except for ( $8 \times 8 \times 8$ ) is an estimation.
9. The real value of Young's modulus of  $\text{CaTiO}_3$  should be extracted by symmetry cells or super cells ( $8 \times 8 \times 8$ ).
10. The value of Young's modulus of  $\text{CaTiO}_3$  extracted with this method can be applied for industrial applications.

**Supplementary Materials:** The following are available online at <https://www.mdpi.com/1996-1944/14/5/1258/s1>, Figure S1: Synthesis route of CaTiO<sub>3</sub>, Table S1: Crystallographic parameters of each individual XRD pattern related to the CaTiO<sub>3</sub>, Figure S2: Linear plot of modified Scherrer equation related to the CaTiO<sub>3</sub>, Figure S3: TEM image of CaTiO<sub>3</sub> powder, Figure S4: Geometry of planes and calculations of planar density of (a) (100), (b) (110), (c) (111), (d) (200), (e) (210), (f) (211), (g) (220), (h) (221), (i) (310), (j) (311) and (k) (222) related to the unit cell of CaTiO<sub>3</sub>, Figure S5: Geometry of planes and calculations of planar density of (a) (100), (b) (110), (c) (111), (d) (200), (e) (210), (f) (211), (g) (220), (h) (221), (i) (310), (j) (311) and (k) (222) related to the super cells (2 × 2 × 2) of CaTiO<sub>3</sub>, Figure S6: Geometry of planes and calculations of planar density of (a) (100), (b) (110), (c) (111), (d) (200), (e) (210), (f) (220), (g) (310) (4 × 4 × 4) and (h) (310) (8 × 8 × 8) related to the super cells (8 × 8 × 8) of CaTiO<sub>3</sub>, Figure S7: Geometry of planes and calculations of planar density of (a) (211) super cell (4 × 4 × 4) and (b) (211) super cell (8 × 8 × 8), Figure S8: Geometry of planes and calculations of planar density of (a) (221) super cell (4 × 4 × 4) and (b) (221) super cell (8 × 8 × 8), Figure S9: Geometry of planes and calculations of planar density of (a) (311) super cell (3 × 3 × 3), (b) (311) super cell (4 × 4 × 4) and (c) (311) super cell (8 × 8 × 8), Figure S10: Geometry of planes and calculations of planar density of (a) (222) super cell (3 × 3 × 3), (b) (222) super cell (8 × 8 × 8).

**Author Contributions:** Conceptualization, M.R. and A.P.; methodology, M.R. and S.N.; investigation, A.V. and A.D.; data curation, A.D.; writing—original draft, M.R.; writing—review and editing, S.N. and G.J.; resources, G.J.; supervision and validation A.P. and G.J. All authors have read and agreed to the published version of the manuscript.

**Funding:** This research was funded by a grant No. S-MIP-19-43 from the Research Council of Lithuania.

**Data Availability Statement:** Data supporting the findings of this study are available from the corresponding author upon request.

**Conflicts of Interest:** The authors declare no conflict of interest.

## References

- Atta, N.F.; Galal, A.; El-Ads, E.H. *Peroovskite Nanomaterials-Synthesis, Characterization, and Applications*; Intechopen: London, UK, 2016.
- Reshmi Varma, P.C. Low-dimensional perovskites. In *Peroovskite Photovoltaics: Basic to Advanced Concepts and Implementation*; Elsevier: Amsterdam, The Netherlands, 2018; pp. 197–229. ISBN 9780128129159.
- Nakamura, T.; Sun, P.H.; Shan, Y.J.; Inaguma, Y.; Itoh, M.; Kim, I.N.S.; Sohn, J.H.O.; Ikeda, M.; Kitamura, T.; Konagaya, H. On the perovskite-related materials of high dielectric permittivity with small temperature dependence and low dielectric loss. *Ferroelectrics* **1997**, *196*, 205–209. [[CrossRef](#)]
- Wang, X.; Xu, C.N.; Yamada, H.; Nishikubo, K.; Zheng, X.G. Electro-mechano-optical conversions in Pr<sup>3+</sup>-doped BaTiO<sub>3</sub>-CaTiO<sub>3</sub> ceramics. *Adv. Mater.* **2005**, *17*, 1254–1258. [[CrossRef](#)]
- Ma, Y.Z.; Sobernheim, D.; Garzon, J.R. Glossary for Unconventional Oil and Gas Resource Evaluation and Development. In *Unconventional Oil and Gas Resources Handbook: Evaluation and Development*; Elsevier Inc.: Amsterdam, The Netherlands, 2016; pp. 513–526. ISBN 9780128025369.
- Slaughter, W.S. *The Linearized Theory of Elasticity*; Birkhäuser Boston: New York, NY, USA, 2002.
- Kuma, S.; Woldemariam, M.M. Structural, Electronic, Lattice Dynamic, and Elastic Properties of SnTiO<sub>3</sub> and PbTiO<sub>3</sub> Using Density Functional Theory. *Adv. Condens. Matter Phys.* **2019**, *2019*. [[CrossRef](#)]
- Nakamura, M. Elastic constants of some transition- metal- disilicide single crystals. *Metall. Mater. Trans. A* **1994**, *25*, 331–340. [[CrossRef](#)]
- Paszkiwicz, T.; Wolski, S. Elastic properties of cubic crystals: Every's versus Blackman's diagram. *J. Phys. Conf. Ser.* **2008**, *104*, 012038. [[CrossRef](#)]
- Ching, W.Y.; Rulis, P.; Misra, A. Ab initio elastic properties and tensile strength of crystalline hydroxyapatite. *Acta Biomater.* **2009**, *5*, 3067–3075. [[CrossRef](#)]
- Holec, D.; Friák, M.; Neugebauer, J.; Mayrhofer, P.H. Trends in the elastic response of binary early transition metal nitrides. *Phys. Rev. B-Condens. Matter Mater. Phys.* **2012**, *85*, 64101. [[CrossRef](#)]
- Knowles, K.M.; Howie, P.R. The Directional Dependence of Elastic Stiffness and Compliance Shear Coefficients and Shear Moduli in Cubic Materials. *J. Elast.* **2015**, *120*, 87–108. [[CrossRef](#)]
- Stair, K.; Liu, J.; Asta, M. Undefined Ultra-sonic measurement and computation of elastic constants. In Proceedings of the ASEE Annual Conference and Exposition, Kansas City, MO, USA, 13–15 September 2006.
- Kelly, A.; Knowles, K.M. *Crystallography and Crystal Defects*; John Wiley & Sons, Ltd.: Chichester, UK, 2012; ISBN 9781119961468.
- Epp, J. X-ray Diffraction (XRD) Techniques for Materials Characterization. In *Materials Characterization Using Nondestructive Evaluation (NDE) Methods*; Elsevier Inc.: Amsterdam, The Netherlands, 2016; pp. 81–124. ISBN 9780081000571.



16. Badawi, F.; Villain, P. Stress and elastic-constant analysis by X-ray diffraction in thin films. *J. Appl. Crystallogr.* **2003**, *36*, 869–879. [[CrossRef](#)]
17. Waseda, Y.; Matsubara, E.; Shinoda, K. *X-ray Diffraction Crystallography X-ray Diffraction Crystallography Introduction, Examples and Solved Problems*; Springer: Berlin/Heidelberg, Germany, 2011.
18. Dong, W.; Song, B.; Meng, W.; Zhao, G.; Han, G. A simple solvothermal process to synthesize CaTiO<sub>3</sub> microspheres and its photocatalytic properties. *Appl. Surf. Sci.* **2015**, *349*, 272–278. [[CrossRef](#)]
19. Wang, Y.; Niu, C.G.; Wang, L.; Wang, Y.; Zhang, X.G.; Zeng, G.M. Synthesis of fern-like Ag/AgCl/CaTiO<sub>3</sub> plasmonic photocatalysts and their enhanced visible-light photocatalytic properties. *RSC Adv.* **2016**, *6*, 47873–47882. [[CrossRef](#)]
20. *ASTM E797—95 Standard Practice for Measuring Thickness by Manual Ultrasonic Pulse-Echo Contact Method*; ASTM International: West Conshohocken, PA, USA, 2001.
21. *ASTM E214—05 Standard Practice for Immersed Ultrasonic Testing by the Reflection Method Using Pulsed Longitudinal Waves*; ASTM International: West Conshohocken, PA, USA, 2007.
22. Sahoo, S.; Parashar, S.K.S.; Ali, S.M. CaTiO<sub>3</sub> nano ceramic for NTCR thermistor based sensor application. *J. Adv. Ceram.* **2014**, *3*, 117–124. [[CrossRef](#)]
23. Cockayne, E.; Burton, B.P. Phonons and static dielectric constant in CaTiO<sub>3</sub> from first principles. *Phys. Rev. B-Condens. Matter Mater. Phys.* **2000**, *62*, 3735–3743. [[CrossRef](#)]
24. Janusas, T.; Urbaitė, S.; Palevicius, A.; Nasiri, S.; Janusas, G. Biologically Compatible Lead-Free Piezoelectric Composite for Acoustophoresis Based Particle Manipulation Techniques. *Sensors* **2021**, *21*, 483. [[CrossRef](#)] [[PubMed](#)]
25. Rabiei, M.; Palevicius, A.; Monshi, A.; Nasiri, S.; Vilkauskas, A.; Janusas, G. Comparing Methods for Calculating Nano Crystal Size of Natural Hydroxyapatite Using X-ray Diffraction. *Nanomaterials* **2020**, *10*, 1627. [[CrossRef](#)]
26. Li, Y.; Thompson, R.B. Relations between elastic constants C<sub>ij</sub> and texture parameters for hexagonal materials. *J. Appl. Phys.* **1990**, *67*, 2663–2665. [[CrossRef](#)]
27. Huntington, H.B. The Elastic Constants of Crystals. *Solid State Phys.-Adv. Res. Appl.* **1958**, *7*, 213–351.
28. De Jong, M.; Chen, W.; Angsten, T.; Jain, A.; Notestine, R.; Gamst, A.; Sluiter, M.; Ande, C.K.; Van Der Zwaag, S.; Plata, J.J.; et al. Charting the complete elastic properties of inorganic crystalline compounds. *Sci. Data* **2015**, *2*, 150009. [[CrossRef](#)]
29. Tariq, S.; Ahmed, A.; Saad, S.; Tariq, S. Structural, electronic and elastic properties of the cubic CaTiO<sub>3</sub> under pressure: A DFT study. *AIP Adv.* **2015**, *5*, 077111. [[CrossRef](#)]
30. Sakhya, A.P.; Maibam, J.; Saha, S.; Chanda, S.; Dutta, A.; Sharma, B.I.; Thapa, R.; Sinha, T. Electronic structure and elastic properties of ATiO<sub>3</sub> (A = Ba, Sr, Ca) perovskites: A first principles study. *IJPAP* **2015**, *53*, 102–109.
31. Wang, H.; Prendiville, P.L.; McDonnell, P.J.; Chang, W.V. An ultrasonic technique for the measurement of the elastic moduli of human cornea. *J. Biomech.* **1996**, *29*, 1633–1636. [[CrossRef](#)]
32. Bray, D.E.; Stanley, R.K. *Nondestructive Evaluation: A Tool in Design, Manufacturing and Service*; CRC press: Boca Raton, FL, USA, 1996.
33. Figliola, R.S.; Beasley, D.E. *Theory and Design for Mechanical Measurements*, 7th ed.; John Wiley & Sons: Hoboken, NJ, USA, 2019.
34. Rabiei, M.; Palevicius, A.; Dashti, A.; Nasiri, S.; Monshi, A.; Vilkauskas, A.; Janusas, G. Measurement Modulus of Elasticity Related to the Atomic Density of Planes in Unit Cell of Crystal Lattices. *Materials* **2020**, *13*, 4380. [[CrossRef](#)]
35. Ramírez, M.A.; Parra, R.; Reboredo, M.M.; Varela, J.A.; Castro, M.S.; Ramajo, L. Elastic modulus and hardness of CaTiO<sub>3</sub>, CaCu<sub>3</sub>Ti<sub>4</sub>O<sub>12</sub> and CaTiO<sub>3</sub>/CaCu<sub>3</sub>Ti<sub>4</sub>O<sub>12</sub> mixture. *Mater. Lett.* **2010**, *64*, 1226–1228. [[CrossRef](#)]
36. Papaconstantopoulos, D.A.; Mehl, M.J. Tight-Binding Method in Electronic Structure. In *Encyclopedia of Condensed Matter Physics*; Elsevier Inc.: Amsterdam, The Netherlands, 2005; pp. 194–206. ISBN 9780123694010.
37. Zhang, J.M.; Zhang, Y.; Xu, K.W.; Ji, V. Young's modulus surface and Poisson's ratio curve for cubic metals. *J. Phys. Chem. Solids* **2007**, *68*, 503–510. [[CrossRef](#)]
38. Mason, W.P. Effect of Dislocations on Ultrasonic Wave Attenuation in Metals. *Bell Syst. Tech. J.* **1955**, *34*, 903–942. [[CrossRef](#)]
39. Reed-Hill, R.E.; Abbaschian, R. *PHYSICAL METALLURGY PRINCIPLES*; Boston PWS Publishing Company: Boston, MA, USA, 2009; ISBN 978-0-495-08254-5.
40. Berdichevsky, V. Energy of dislocation networks. *Int. J. Eng. Sci.* **2016**, *103*, 35–44. [[CrossRef](#)]
41. Hull, D.; Bacon, D.J. *Introduction to Dislocations*, 5th ed.; Butterworth-Heinemann: Burlington, MA, USA, 2011; ISBN 9780080966724.
42. Englert, U. Symmetry Relationships between Crystal Structures. Applications of Crystallographic Group Theory in Crystal Chemistry. By Ulrich Müller. *Angew. Chem. Int. Ed.* **2013**, *52*, 11973. [[CrossRef](#)]
43. Duparc, O.H.; Polytechnique, É.; Duparc, O.B.M.H. A review of some elements in the history of grain boundaries, centered on Georges Friedel, the coincident “site” lattice and the twin index Crystallography History View project ANR FluTi View project A review of some elements in the history of grain boundaries, centered on Georges Friedel, the coincident “site” lattice and the twin index. *Artic. J. Mater. Sci.* **2011**, *46*, 4116–4134.